PAPER

Check for updates

Unusually high spin–orbit coupling in the methionine singlet–triplet transition and the role of magnetic perturbations in amino acids†

B. Minaev, [ID] *[ab] M. Sukhyna, [ID] [a] P. Stakhira,[d] V. Minaeva[a] and H. Ågren [ID] [bc]

Forbidden triplet–singlet transitions ($T_1 \leftarrow S_0$) in a few amino acids (methionine, glycine, tryptophan, cysteine) have been examined for their possible detection. This computational study is based on time-dependent density functional theory (TD-DFT) with spin–orbit coupling (SOC) account. The results of this study indicate that the possibility of detecting the absorption $T_1 \leftarrow S_0$ band is quite high for methionine and cysteine. The results demonstrate that the presence of sulfur in amino acids enhances the SOC effect, increasing the intensity of the singlet–triplet absorptions up to a measurable extinction coefficient. The importance of these SOC effects on the photochemical properties of proteins is emphasized together with the potential role of triplet–singlet transitions in photobiology.

Introduction

The term "methionine triplet" is well-known in molecular genetics. In this study, we propose a new additional assonance to "methionine triplet." We are referring to the triplet excited state of the methionine molecule, which has not been previously reported based on its particular properties, which were revealed using experimental measurements. Methionine, similar to all other amino acids, possesses a singlet ground state (S_0) and a lowest excited molecular triplet (T_1) state. These states are typically associated with the phosphorescence phenomena (radiative $T_1 \rightarrow S_0$ transition) usually observed in viscous or solid solutions.[1] The energy of the triplet T_1 state is lower than that of the singlet excited S_1 state, which produces a fast fluorescence emission in the $S_1 \rightarrow S_0$ transition after light absorption. The T_1 state is also responsible for the delayed emission, which is known to be of the P and E types according to Parker's discoveries;[2] the late phenomena are now renamed as thermally activated delayed fluorescence (TADF).[1] Similar to all aliphatic

amino acids, the methionine molecule absorbs light in the UV region in the form of a wide absorption band (150–250 nm), with a maximum at the middle of the interval, but never exhibits phosphorescence.[3–5] The present results shed light on the possible role of the methionine triplet in the photo- and radio-biology of proteins.[5–9]

Within the field of molecular spectroscopy, the term "triplet" is used to determine the total electronic spin state of a molecule. The electronic wave function Ψ must be an eigenfunction of the $\vec{S}^2$ and S_z operators, where $\vec{S} = \sum_i \vec{s}_i$ is the total spin operator (eqn (1)).

$$\vec{S}^2\Psi = S(S+1)\hbar^2\Psi; \quad S_z\Psi = M_S\hbar\Psi \tag{1}$$

In the triplet state, the total spin quantum number of a molecule is equal to $S = 1$. This provides three possible spin projections in the external magnetic field direction (z-axis). These correspond to three values of the spin magnetic quantum number M_S, which can be -1, 0, or 1. In the ground state of a diamagnetic molecule, the spin quantum number is zero ($S = 0$), indicating that all electron spins quench each other by being paired on the occupied molecular orbitals (MO) according to the Pauli principle. This introduction completes our etymological explanation on the genetic term "methionine triplet" and presents a new perspective on its role in photobiology.

Light absorption by molecules typically leads to the observation of the singlet–singlet $S_0 \rightarrow S_n$ transitions, which are allowed by the spin selection rule in the electric dipole approximation.[1] In contrast, the singlet–triplet $S_0 \rightarrow T_n$ transitions are spin-forbidden, resulting in their zero intensity, solving the Schrödinger equation without spin–orbit coupling

[a] Cherkasy National University named after Bogdan Khmelnytsky, Institute of Natural and Agricultural Sciences, Cherkasy, Cherkasy Oblast, Ukraine. E-mail: bfmin43@uke.net

[b] Uppsala Universitet, Department of Physics and Astronomy, Uppsala, Uppsala County, Sweden

[c] Wroclaw University of Science and Technology, Faculty of Chemistry, Wrocław, PL-50370, Poland

[d] Lviv Polytechnic National University Institute of Telecommunications Radioelectronics and Electronic Engineering, Department of Electronic Engineering, Lviv, Lviv Oblast, Ukraine

(SOC) account. In fact, the $S_0 \rightarrow T_1$ transitions in organic molecules are observed with a long optical path because of their low intensity.[1] To calculate such absorption, the SOC must also be included. In this case, the values of S and M_S in eqn (1) are not good quantum numbers; despite this fact, the full wave function is still antisymmetric with respect to the permutation of any pair of electrons and satisfies Pauli's principle. Consequently, the energies of the S_1 and T_1 states in these cases will be different. S–T splitting occurs even when the potential energy operator does not account for magnetic interactions that depend on spin. The reason is connected to the exchange interaction, which depends on the permutational symmetry of the orbital and spin parts of the wave function.

Since the first excited state of an ordinary organic diamagnetic molecule is always a spin triplet T_1 state, its role in organic photochemistry and spectroscopy is very important, despite the spin-prohibition of the $S_0 \rightarrow T_1$ transitions.[1] Such transitions are induced by internal magnetic interaction –spin–orbit coupling (SOC) in molecules, which allows S–T states with different spin multiplicities to mix according to the rule ($\Delta S = \pm 1$). It is worth noting that SOC effects are much stronger in amino acids than in most typical organic compounds containing no heavy atoms.[1] This is due to the presence of carboxylic and amino groups in proteins, which have n-orbitals of lone pairs and mixed σ–π MO wave functions. SOC depends strongly on the atomic nuclear charge Z (as Z^4), but the change in orbital angular momentum during an S–T transition is also very important for the spectral manifestations of the SOC effects.

Compounds containing either carbonyl or amino groups individually play an important role in the conceptual understanding of organic photochemistry and spectroscopy because of the typical σ–π and n-orbital separation in many such chromophores, where SOC influences the luminescent properties, it is easily classified by the El-Said rules.[1,9] With particular attention to the excited triplet state behavior, these rules thus explain the luminescence of many organic chromophores with π and n electrons. As far as proteins are concerned, only amino acids that contain aromatic cite groups are mentioned in this context.[1,3–6] We note that the role of SOC perturbations and triplet states properties of aliphatic amino acids are rarely discussed in the photobiology and spectroscopy of proteins.[1,3]

Amino acid spectroscopy

The electronic absorption spectra of proteins and individual amino acids in aqueous solutions exhibit broad $S_0 \rightarrow S_n$ bands within the ultraviolet region (150–280 nm). The longest wavelengths and distinctive absorptions observed in the protein spectra by standard non-vacuum spectrophotometers are attributed mainly to non-saturated chromophores present in the side chains of aromatic amino acids; this concerns tryptophan (absorption peak at approximately 280 nm, molar extinction coefficient of $\varepsilon = 5600$ M^{-1} cm^{-1}) and tyrosine (peak at 275 nm, $\varepsilon = 1420$ M^{-1} cm^{-1}).[3] The aromatic residues undergo π–π* transitions under UV absorption and then release photons,

emitting fluorescence at longer wavelengths (about 360 nm) than the absorption maximum.

Peptide bonds in proteins typically exhibit a strong absorption peak around 190 nm ($\varepsilon = 7000$ M^{-1} cm^{-1}) and a relatively weak absorption in the region 210–220 nm ($\varepsilon = 100$ M^{-1} cm^{-1}), with a gradual decrease in intensity at longer wavelengths. A relatively low level of absorption has been reported for protein transitions, with an oscillator strength (f) of approximately $f = 10^{-5}$.[3] The weak UV absorption of the disulfide bonds in cystine is also well known and can be observed in the wide region of 250–320 nm. Therefore, proteins that do not contain aromatic amino acids or disulphide bonds will be practically transparent at wavelengths above 250 nm.[3]

Upon UV light illumination and absorption, the amino acid molecule undergoes non-radiative $S_n \rightarrow S_1$ transitions (internal conversion, IC) and subsequent $S_1 \rightarrow T_1$ intersystem crossing (ISC) processes.[4–8] The ISC relaxation competes with fast fluorescence ($S_1 \rightarrow S_0$ radiative transitions), which has been observed for tryptophan, tyrosine and many green fluorescent proteins (GFP).[5] The fluorescence spectrum and its lifetime are very sensitive to changes in the protein's secondary structure because of the IC and ISC relaxation mechanisms and energy transfer to the nearest nano-environment.[6]

The generation of triplet T_1 states upon illumination of GFP is well known; they are commonly populated via ISC processes.[5–7] The typical quantum yield of triplets in GFP and other organic dyes is about 10^{-3}, but they are effectively quenched by the triplet oxygen dissolved in tissues.[5] The observable lifetimes of triplets in anaerobic conditions are up to milliseconds; however, they are much shorter in the presence of $O_2(^3\Sigma^-)$.[1,8] Triplet lifetimes of 10–40 μs have been measured at normal aerobic conditions for selected fluorescent proteins (eGFP mutants[6]); such relatively long T_1 state lifetimes are explained by the protective role of transmembrane β-barrel proteins.[5,6] For many organic days and benzene derivatives, the calculated triplet radiative lifetimes are much longer (about 10–100 s).[9,10] Information on fluorescence and phosphorescence of individual aliphatic amino acids is, however, absent. Probably, the S_1 and T_1 excited states of these molecules are effectively quenched by intermolecular energy transfer because their high excitation energy (~ 5 eV) can be easily donated to many acceptors (vibronic states of surrounding molecules with lower excited state energies). For amino acid delayed fluorescence, neither P nor E-type[2] has been reported thus far.

The fate of the «dark» T_1 state in aliphatic amino acids has not attracted the attention of photobiologists and its role in protein photochemistry remains unknown.[1,3–5] The transient intermediates formed in the IC and ISC radiationless processes are still «dark» and not amenable to detection by ordinary light absorption or emission.[1,3,4] However, these dark intermediates play critical roles in IC and ISC processes, including fluorescence quenching, and thus are essential for understanding the mechanistic photochemistry of proteins with the standard flash-photolysis methods.

Recently, L-methionine has been used for the determination of Cu^{2+} and Co^{2+} ions based on their quenching effect on the

orange fluorescence (580 nm) of methionine-capped gold nanoclusters (Met-AuNCs).[11] In the cluster preparation L-methionine was used as a reducing and protecting reagent. It also participates in the interaction with Cu^{2+} and Co^{2+} ions, assisting in the photoinduced electron transfer (PET) and the aggregation-induced quenching of the Met-AuNCs cluster fluorescence (580 nm).[11]

Looking ahead, it is interesting to note that the present TD-DFT calculation of the optimized T_1 state of methionine predicts a $T_1 \rightarrow S_0$ emission with a shorter wavelength of 562.3 nm and a relatively short radiative lifetime of 10 ms.

Fifteen years ago, we calculated the singlet–triplet transition intensity in the long-wave absorption tail of the glycine anion NH_2–CH_2–COO^- in an alkaline solvent at high pH > 9.[1,4] Our SOC calculations using the quadratic response method[4,9] provided a relatively high oscillator strength for the $S_0 \rightarrow T_1$ transition at 241 nm ($f = 0.51 \times 10^{-6}$). The T_1 state exhibits $^3A''$ spatial symmetry with respect to reflection in the OCO–CN atomic plane of the glycine anion.[4]

The second T_2 triplet in this anion is the totally symmetrical $^3A'$ state; the calculated wavelength (220 nm) of the $S_0 \rightarrow T_2$ transition coincides with the more intense offset of the singlet–singlet absorption of the glycine anion. At the same time, the calculated oscillator strength for the $S_0 \rightarrow T_2$ transition ($f = 0.44 \times 10^{-4}$) is comparable with the spin-allowed singlet–singlet $S_0 \rightarrow S_1$ transition. For example, the $S_0 \rightarrow T_n$ absorption of aromatic hydrocarbons is five-six orders of magnitude weaker.[1,10] These results indicate that relativistic effects are important for near-UV light absorption by the simple amino acids. We cannot exclude the possibility that similar effects may be important for polypeptides and real proteins. Thus, radiation damage to simple amino acids, like glycine, can be induced at longer wavelengths than what has generally been accepted and what is known from their typical absorption spectra detected by standard spectrophotometers.[4–6]

Computational details

Time-dependent density functional theory (TD-DFT) is a powerful and widely used approach for quantum chemical calculations of molecular spectra.[12] Decades ago, our research group predicted, on the basis of TD-DFT calculations with SOC account,[1,4] the potential for weak absorption at the low-frequency edge in the region of 240–260 nm of a few simple amino acids associated with the vertical $S_0 \rightarrow T_1$ transitions.

In our calculations, we used the TD-DFT method with the B3LYP functional[13] and the 6-311++G(d,p) basis set,[14] accounting for spin–orbit coupling in the Orca 5.0.4 software package.[12] As noted above, the triplet–singlet transitions are forbidden in the non-relativistic approximation, but the SOC perturbation mixes states with different multiplicities, which gives rise to a non-zero transient dipole moment described by perturbation theory.[1,10] Let us briefly examine the theoretical aspects of such calculations.

The electric dipole S_0–T_1 transition moment, which is associated with the spin sublevel a, is determined by the following equation:

$$M_{T-S} = \left\langle \tilde{S}_0 \left| \sum_i er_i \right| \tilde{T}_1^a \right\rangle = \sum_n \frac{\langle S_0 | \sum_i er_i | S_n \rangle \langle S_n | \hat{H}_{SO}^a | T_1^a \rangle}{E(T_1) - E(s_n)}$$
$$+ \sum_m \frac{\langle S_0 | \hat{H}_{SO}^a | T_m^a \rangle \langle T_m^a | \sum_i er_i | T_1^a \rangle}{E(s_0) - E(T_m)},$$

(2)

where $\hat{H}_{SO}^a$ is the a-component of the SOC operator ($a = x, y, z$) and r_i is the radius vector of the i-electron. The a-axes determine the M_S sublevel quantization in the absence of an external magnetic field and the so-called zero-field splitting (ZFS) energy of the T^a sublevel.[15,16] The ZFS energy is determined by the spin–spin coupling of two non-paired electrons and by SOC – in the second order of perturbation theory.[10] In general, the ZFS parameters of a triplet-excited molecule depend on the solvent;[16] however, we neglect this dependence in the present study.

Due to the SOC effect, the triplet states of a molecule have admixtures of singlet state wave functions, which can be described by first-order perturbation theory. Hence, the wave function of the perturbed $\tilde{T}_1$ state can be represented as a zero-order T_1 wave function and an impurity of the n-singlet states S_n.

$$\tilde{T}_1 = T_1 + \sum_n \frac{\langle S_n | H_{SO} | T_1 \rangle}{E(T_1) - E(S_n)} S_n$$

(3)

Thus, the larger the SOC integral and the smaller the energy gap $E(T_1) - E(S_n)$ in the denominator, the greater the value of the singlet impurity. After submission eqn (3) into the transition moment $\left\langle \tilde{S}_0 \left| \sum_i er_i \right| \tilde{T}_1^a \right\rangle$ one obtains directly the left part of eqn (2). If we take $n = 0$ and $m = 1$ in eqn (2), the simple contribution from the difference in the permanent electric dipole moments of the S_0 and T_1 states occurs as follows:

$$M_{T-S} = \frac{\langle S_0 | \sum_i er_i | S_0 \rangle \langle S_0 | \hat{H}_{SO}^a | T_1^a \rangle}{E(T_1) - E(S_0)} + \frac{\langle S_0 | \hat{H}_{SO}^a | T_1^a \rangle \langle T_1^a | \sum_i er_i | T_1^a \rangle}{E(S_0) - E(T_1)}$$
$$= (\mu_0 - \mu_T) \frac{\left\langle \tilde{S}_0 \left| \sum_i er_i \right| \tilde{T}_1^a \right\rangle}{E(T_1) - E(S_0)}$$

(4)

For the SOC calculation, we used the full form of the Breit–Pauli operator given by the following equation:[9]

$$\hat{H}_{SO} = \frac{e^2 \hbar^2}{2m^2 c^2} \left[\sum_{i,A} Z_A \frac{l_{iA} \cdot s_i}{r_{iA}^3} - \sum_{i,j} \frac{l_{ij} \cdot (s_i + 2s_j)}{r_{ij}^3} \right],$$

(5)

where the indices i, j refer to electrons, the index A – to nuclei, Z is the charge of the nucleus, l and s are the orbital and spin angular momentum operators, respectively.[9]

In general, this operator provides very accurate SOC constants for orbitally degenerate L–S states in light atoms and diatomic molecules and determines the energy level splitting of the spin multiplets.[9] For non-linear polyatomic molecules, the orbital angular momentum is quenched and the expectation

13342 | *Phys. Chem. Chem. Phys.*, 2025, **27**, 13340–13351

This journal is © the Owner Societies 2025

Paper

PCCP

value of the SOC operator is zero. Thus, the direct SOC contribution to the zero-field splitting of the molecular triplet sublevels vanishes.[9] The SOC energy in this case is not measurable; it influences the observable S–T transition intensity through the imaginary SOC matrix elements in eqn (2).

This makes it possible to accurately calculate the energies and probabilities of S–T transitions, which is crucial for understanding the spectral properties and kinetic behavior of such systems. An important characteristic of electronic S–T transitions is the oscillator strength f, which is proportional to the square of the electro-dipole transition moment (M_{S-T}).

$$f_{S-T} = \frac{2}{3}\Delta E M_{S-T}{}^2, \qquad (6)$$

where $M_{S-T}{}^2 = \sum_\alpha \sum_\gamma \left| \left\langle \tilde{S}_0 \middle| M_\gamma \middle| \tilde{T}_1^\alpha \right\rangle \right|^2$, M and ΔE values are in atomic units (a.u.), and f – is a dimensionless value.

Knowing the electro-dipole moment of the S–T transition, we can find the radiative lifetime τ_a of the excited triplet state, which is inversely proportional to the radiative rate constant (k_a) of the $S_0 \leftarrow T_1{}^a$ transition:

$$k_\alpha = \frac{1}{\tau_\alpha} = \frac{64\pi^4 (\Delta E_{T-S})^3}{3h^4 c^3} \sum_\gamma {}^{x,y,z} \left| M_\gamma(T_1^\alpha) \right|^2 \qquad (7)$$

It is crucial to know the lifetime of an excited triplet state to understand the photochemical behavior of a substance because this can affect the way of possible photochemical reactions and purely physical energy-transfer processes. Given the potential influence of weak $S_0 \rightarrow T_1$ transitions on the generation of long-lived triplet states, which may, in turn, affect photochemical transformations (including the decay of individual amino acids) during their lifetimes in proteins, a detailed analysis of the spin–orbit coupling in proteins is required. The results of our quantum chemical calculations of the spectra of a few amino acids accounting for the spin–orbit coupling are presented below.

Results and discussion

As discussed previously, methionine is a vital amino acid essential for the survival of all eukaryotes and their genetic evolution. Methionine exists in two different hirable structures: L and D species. Despite the differing spatial structures, the two forms exhibit identical mirroring of their atomic arrangement.[3] In the context of biochemical processes, L-isomers assume a more significant role because of evolutionary adaptations of biological systems that have enabled enzymes to recognize and utilize L-isomers. Conversely, D-isomers are less prevalent in living organisms, largely due to their spatial structure not aligning with the specific configuration of enzyme active sites. Consequently, their involvement in biochemical processes is predominantly limited and, in some cases, deleterious.

Before investigating electronic transitions, the amino acids selected for this study were optimized using the ORCA code[12] by density functional theory (DFT) method with B3LYP functional[13] and the 6-311++G(d,p) basis set.[14] The optimized
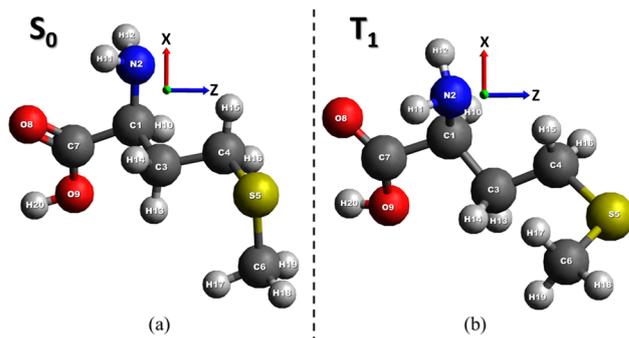

Fig. 1 Optimized geometry of the ground S_0 state (a) and the first excited state T_1 (b) of L-methionine.

geometry of L-methionine in the ground S_0 state illustrated in Fig. 1a, is in good accordance with the experimental data presented in the reference.[17] The triplet T_1 state optimization is obtained by the time-dependent (TD) DFT approach.[12] Tables S1 and S2 (ESI†) provide a comprehensive overview of the geometric parameters of methionine in the ground S_0 and excited T_1 states.

The general backbone structure of the carboxylic and amino groups attached to the saturated carbon C1 atom (Fig. 1) is reflected in the common features of the gas-phase microwave, IR, UV, and X-ray absorption spectra of many amino acid C edge NEXAFS spectra.[7,17]

The obtained geometry was used to calculate the electronic absorption spectra by considering the SOC perturbation and vibrational modes into account. Vibronic analysis of normal coordinates on the potential energy surface (PES) of the L-methionine molecule can be started with the Duschinsky transformation for the electronic S–T transition between two PES varieties:[1] $Q_T = JQ_S + D$, where Q_T and Q_S are the mass-weighted normal coordinate matrices of the triplet T and singlet S states obtained by DFT gradient minimization and finding vibration frequencies, J is the Duschinsky's rotation matrix determining transformation of the T and S state's coordinate systems, and D is the matrix of displacement vector presenting in detail the geometry changes between T and S states, which are partly shown in Tables S1 and S2 (ESI†). These matrix transformations allow the calculation of the Huang–Rhys parameters and the Franck–Condon factors for vibronic transitions.[18,19] Upon $S_0 \rightarrow T_1$ excitation, the whole carboxyl group undergoes strong deformation and prolongation of all chemical bonds (Table S1, ESI†); the C=O and C–OH bond lengths increase by 0.065 and 0.111 Å, respectively. From Table 1, we can see that this excitation is produced simultaneously by two HOMO $\rightarrow$ LUMO and HOMO $\rightarrow$ LUMO+2 electronic configurations.

The first one corresponds to the charge-transfer (CT) transition from the sulfide to the carboxyl group; moreover, the LUMO is an antibonding orbital with respect to the O=C–O moiety (Fig. 2).

This also explains the drastic change in the carboxyl plane orientation with respect to the quasi-planar carbon zig-zag

This journal is © the Owner Societies 2025

Phys. Chem. Chem. Phys., 2025, **27**, 13340–13351 | **13343**

Table 1 Characteristics of the vertical electronic transitions of L-methionine in the ground-state geometry (absorption)

Transition	λ, nm	f	Contribution of orbitals to the transition	ΔE_{vert}, eV
$S_0 \rightarrow T_1$	260.6	2.76×10^{-6}	HOMO $\rightarrow$ LUMO (36.29%)	4.757
			HOMO $\rightarrow$ LUMO+2 (35.67%)	
$S_0 \rightarrow T_2$	251.7	1.51×10^{-5}	HOMO $\rightarrow$ LUMO+1 (46.28%)	4.927
			HOMO $\rightarrow$ LUMO+2 (22.36%)	
$S_0 \rightarrow S_1$	249.1	2.07×10^{-2}	HOMO $\rightarrow$ LUMO (74.45%)	4.976
			HOMO $\rightarrow$ LUMO+2 (24.55%)	
$S_0 \rightarrow S_2$	245.6	1.40×10^{-2}	HOMO $\rightarrow$ LUMO+1 (90.14%)	5.048
$S_0 \rightarrow S_3$	238.5	1.37×10^{-2}	HOMO $\rightarrow$ LUMO+2 (57.18%)	5.199
$S_0 \rightarrow S_4$	228.3	1.35×10^{-2}	HOMO $\rightarrow$ LUMO+3 (66.02%)	5.431
$S_0 \rightarrow S_6$	217.6	3.34×10^{-2}	HOMO $\rightarrow$ LUMO+4 (80.84%)	5.697

chain; the dihedral angle $\angle$(O8=C7–C1–C3) changes by 73.37°. Even larger angular deformation undergoes the sulfide group; see the angle $\angle$(C3–C4–S5–C6) in Table S2 (ESI†). At the same time, both C–S bonds experience a large reduction (about 0.03 Å) at the $S_0 \rightarrow T_1$ transition since the excited electron leaves the C–S–C antibonding HOMO orbital (Fig. 2). The same force-field change supports the second electronic configuration HOMO $\rightarrow$ LUMO+2, which represents the excitation of the sulfide group. To some extent, this is a local n–σ* transition at the sulfur atom (see HOMO $\rightarrow$ LUMO+2 in Fig. 2).

Thus, the highest occupied MO of L-methionine represents a typical lone pair of electrons at the $3p_z$ AO of the sulfur atom, conjugated with the nearest carbon $2p_z$ orbitals, and the lowest T_1 excited state is produced by a single electron excitation from this lone pair to σ*(C–S) and to π*(C=O) antibonding orbitals. The vertical $S_0 \rightarrow T_1$ transition of the L-methionine molecule in the gas phase is expected to be relatively intense (Table 1) in comparison with the aromatic tryptophan counterpart (Table S3, ESI†). A similar SOC approach with a quadratic response calculation predicts for benzene derivatives much weaker $S_0 \rightarrow T_1$ absorption.[10] Only Br-benzene has an oscillator strength of about 10^{-8}, and all other molecules without heavy atoms show $f \approx 10^{-10}$; it is interesting that the $S_0 \rightarrow T_2$ absorption in the studied benzene derivatives was predicted to be about an order of magnitude more intense than the first

$S_0 \rightarrow T_1$ transition.[10] The same trend was observed for the L-methionine molecule (Table 1), although its S–T transition intensities were four orders of magnitude higher than those of aniline, styrene and indole.[10] Thus, we propose that the $S_0 \rightarrow T_1$ absorption at the long-wavelength wing of L-methionine (260 nm) can be detected by the Zeeman effect and EPR spectra.

According to our DFT calculations of the L-methionine singlet S_0 state geometry optimization, the vertical $S_0 \rightarrow T_1$ absorption is predicted at 260.6 nm with an oscillator strength $f = 2.76 \times 10^{-6}$ (Table 1). In this Table, we present the first two triplet states and the number of singlet transitions of L-methionine. The lowest excited states, T_1 and T_2, lie in the range of 250–260 nm. As illustrated in Table 1, all these excitations can be attributed to the transitions from the highest occupied molecular orbital (HOMO), which is mostly localized as the lone pair of electrons of the sulfur atom at the $3p_z$ AO (Fig. 2).

The main contribution to the $S_0 \rightarrow T_1$ transition intensity in L-methionine is determined by the direct SOC mixing of these states, which follows from eqn (4). Table S3 (ESI†) presents the S_0–T_1 SOC matrix elements (ME) for all studied molecules. For sulfur-containing amino acids, these SOC ME values are unusually high (for methionine, it is equal to 117 cm^{-1}, while the S_0 and T_1 states dipole moment are equal to 2.02 and 16.8 Debye, respectively). The T_1 state of methionine includes a large CT contribution. Accounting for the long chain between the S atom and the COOH group, the great dipole moment is obvious, as well as the large contribution of eqn (4) to the $S_0 \rightarrow T_1$ transition intensity in L-methionine.

Usually, the spin-forbidden $S_0 \rightarrow T_1$ transition intensity is borrowed from the spin-allowed singlet–singlet $S_0 \rightarrow S_n$ transitions if the upper singlet state S_n is mixed by SOC ME with the referenced T_1 triplet, eqn (2). Similarly, the ground S_0 state can be perturbed by the highly excited T_m state ($m \neq 1$). In this case, the spin-forbidden $S_0 \rightarrow T_1$ transition borrows its intensity from the allowed $T_1 \rightarrow T_m$ transitions, which are measurable in impulse flash-photolysis experiments.[2] All terms are important in eqn (2) for amino acids because the dense manifold of n–π*, n–σ* and π–π* states with different AO orientations creates an opportunity for intra-atomic orbital angular momentum changes inside carboxyl, amino and sulfide groups, which are important for the SOC ME integrals.[1] The intense SOC mixing between excited S and T states with small energy gaps is important for all amino acids. At the same time, a large energy

40 HOMO (E = −6.051 eV)   41 LUMO (E = −0.449 eV)

41 LUMO+1 (E = −0.437 eV)   42 LUMO+2 (E = −0.437 eV)
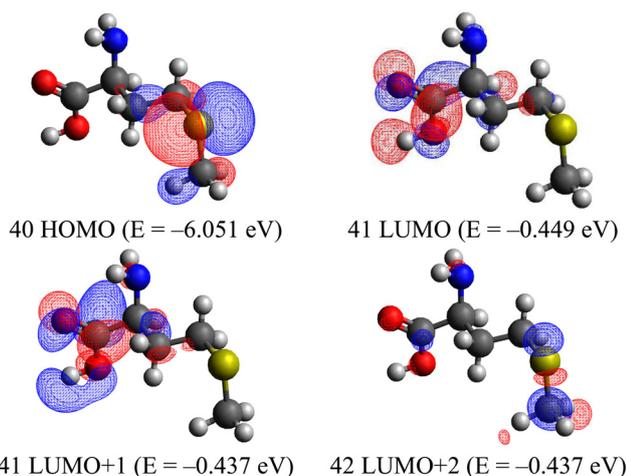
Fig. 2 Some molecular orbitals of L-methionine calculated in the ground-state geometry.

13344 | *Phys. Chem. Chem. Phys.*, 2025, **27**, 13340–13351

This journal is © the Owner Societies 2025

gap ΔE (S_0, T_1) with the ground state in aliphatic amino acids (about 5 eV, Table S1, ESI†) diminishes the role of the second term in eqn (2), as well as a separate contribution of eqn (4). Nevertheless, the great difference in the permanent dipole moments of the S_0 and T_1 states together with unusually large SOC ME provide the largest contribution of eqn (4) to the $S_0 \rightarrow T_1$ transition moment in L-methionine.

All the discussed calculations of the S–T absorption intensity concern the vertical excitations from the optimized ground state, which correspond to the vibrational excited triplet state. Following the Franck–Condon (FC) principle, one can anticipate that the FC factors of such a vibronic band would be close to unity. Account of the large distortion of the carboxyl and sulfide groups upon the $S_0 \rightarrow T_1$ transition (Tables S1 and S2, ESI†) together with the calculated vibrational frequencies allows us to estimate the global FC factor for the 0–0 transition as equal to 0.214. The most distortion in the T_1 state refers to the vibrational mode ν_{23} = 688.9 cm^{-1} (symmetric stretch of the sulfide C–S–C group), and partly – the ν_{24} = 731.6 cm^{-1} mode (asymmetric sulfide C–S–C stretching). The ν_{48} = 1511.6 cm^{-1} mode of the C=O valence vibration includes deformation of the COH bending and a few CH$_2$-bending vibrations. Although the frequency of the corresponding vibrations in the ground state was slightly changed, the forms of the normal modes were similar (Fig. S7, ESI†).

We must note that the T_1 state geometry optimization with the spin unrestricted UB3LYP functional leads to the dissociation of the SCH$_3$ group and only the TD DFT/B3LYP method provides an equilibrium molecular triplet structure. In any case, the T_1 state is not very stable; the triplet dissociation energy calculated using the UB3LYP method is equal to 1.89 eV, whereas in the ground state, it is almost twice as much (3.75 eV).

To present an idea on possible phosphorescence and its 0–0 band, we calculated the radiative transitions of L-methionine in the T_1-state optimized geometry by TD-DFT (Table 2 and Fig. S2, ESI†). We predict visible emission at 562 nm with a radiative lifetime of 2.3 ms as the most intense phosphorescence red wing. This is the vertical emission from the relaxed T_1 state to the excited vibrational level of the ground S_0 state. The total electronic energy of the S_0 and T_1 optimized states of L-methionine is equal to -800.418395 and -800.276433 a.u., respectively; thus, the electronic transition energy is 3.863 eV,

which corresponds to 321 nm. The zero-point energy of vibrations is equal to 0.1650 and 0.1621 a.u., respectively, and we predict the final 0–0 transition energy of 3.782 eV, which corresponds to 328 nm. This should provide an accurate prediction of the 0–0 phosphorescence band. The approximate estimation of the Huang–Rhys (y) and Franck–Condon factors[18,19] for this transition gives τ_r = 350 ms. (For soft modes, we used y factors equal to 0.3).[18] The radiative lifetimes for the most intense vertical emission and the 0–0 band are of the millisecond order. However, the fast non-radiative quenching (NRQ) proceeds thousands of times faster and cannot afford to emit phosphorescent red light. The NRQ rate constant (k_{NR}) estimation according to the method[18] provides a k_{NR} value of 5.7×10^6 s^{-1}. A large internal rotation of the SCH$_3$ group and other distortions between the S_0 and T_1 equilibria (Tables S1 and S2, ESI†) provide effective energy flow to vibrational modes, leading to the phosphorescence quenching of methionine.

The theoretically calculated electronic spectrum of the vertical $S_0 \rightarrow S_n$ transitions of L-methionine (Fig. S1a, ESI†) shows a relatively intense first absorption band with a maximum close to 250 nm (ε = 2000 M^{-1} cm^{-1}) and a series of half-weaker bands in the middle UV region (Table 1). The band half-width in Fig. S1 (ESI†) is equal to 0.61 eV. The same TD-DFT method predicts that L-methionine has a strong absorption band at approximately 217 nm, which corresponds to the $S_0 \rightarrow S_6$ transition involving the sulphur-containing side chain. There was no absorption of methionine in the visible region (Fig. S1a, ESI†) according to experimental data.[2] As can be seen in Table S1 (ESI†), the two $S_0 \rightarrow T_{1,2}$ transitions occurred at the long-wavelength edge of the weak absorption (250–260 nm), which was not contradictory to the experiment.[3] Given the width of the bands, it is possible that they can be overlapped by the $S_0 \rightarrow S_1$ transition.

Absorption spectrum of glycine

The simplest amino acid was studied for comparison with L-methionine spectra. Glycine, as a natural α-amino acid in the gas phase, exists exclusively in a neutral form and represents a rich conformational landscape[17,20,21] which is determined by various types of intramolecular interactions between carboxyl and amino groups. Their competition through different combinations of hydrogen bonds was carefully studied in theory[21]

Table 2 Characteristics of the vertical electronic transitions of L-methionine in the T_1-state geometry (emission)

State	λ, nm	$\tau(T_1)$, s	Oscillator strength, f	Contribution of orbitals to the transition	ΔE, eV
T_1	562.3	0.0023	2.04×10^{-6}	HOMO−1 ← LUMO (1.58%) HOMO ← LUMO (97.66%)	2.205
S_1	554.9	0.000038	1.21×10^{-4}	HOMO ← LUMO (99.44%)	2.235
T_2	396.1	0.00396	5.94×10^{-7}	HOMO−4 ← LUMO (2.04%) HOMO−3 ← LUMO (39.62%) HOMO−2 ← LUMO (30.85%) HOMO−1 ← LUMO (24.27%) HOMO ← LUMO (1.70%)	3.130
S_2	341.5	0.000001	2.27×10^{-3}	HOMO−3 ← LUMO (8.04%) HOMO−2 ← LUMO (6.89%) HOMO−1 ← LUMO (83.83%)	3.631

This journal is © the Owner Societies 2025

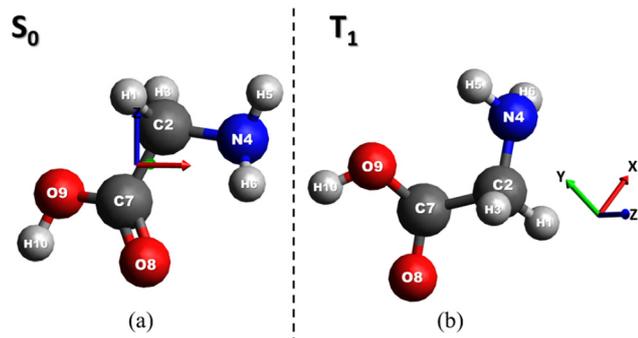Phys. Chem. Chem. Phys., 2025, **27**, 13340–13351 | **13345**

Fig. 3 Optimized structure of the S_0 ground state (a) and T_1 excited state (b) of glycine.

and in experiment.[17] The optimized glycine structures in the ground S_0 state and the first excited T_1 state are illustrated in Fig. 3 and Table S4 (ESI†). In the ground state, almost all the heavy atoms in the chain are in one plane. Only nitrogen atoms deviate from the O=C–O–C plane due to the small dihedral angle of 20.14°, which is equal to the ∠N–C–C=O angle. The deviation of the H_{10} atom is negligible (1.06°); for atom H_6, it is more serious (38.7°). The valence bond angles in the chain were close to 117.5°; only ∠CCN angle deviates to 110.5°. The bond angle ∠H–C–H is equal to 106.4° and the angle ∠H–N–H is 108.9°, which slightly deviates from the sp^3 hybridization parameters. We can approximately assign vertical S_0–S_n transitions of glycine in terms of π–π* and n–π*types, though our optimized structure does not contain a symmetry plane.

In the optimized T_1 state at the TD-DFT level, the heavy atoms in the glycine chain deviate far from the planar structure. The main difference from the ground S_0 state structure is determined by a big out-of-plane deviation of the carboxyl group. The dihedral angle ∠N–C–C=O is equal to 173.073° and close to planarity, while the ∠N–C–C–O angle is equal to (−56.55°). In the ground state, these angles are 20.14° and (−161.89°), respectively. Thus, upon the adiabatic $S_0 \rightarrow T_1$ excitation, an almost planar zig-zag chain of heavy atoms in glycine experiences out-of-plane zig-zag distortion and inversion of the CH_2–NH_2 group (Fig. 3).

Comparing the vertical $S_0 \rightarrow T_1$ transition of methionine with that of glycine (Tables 1 and 3), we can conclude that the former transition is 56 times more intense (in methionine and glycine these transitions possess $f = 2.76 \times 10^{-6}$ and $f = 4.9 \times 10^{-8}$, respectively). The two low-lying singlet excited states at about 5.4 and 5.8 eV (Table 3) are in reasonable agreement with

experiment and theory (5.6 and 5.8 eV).[20] These represent transitions with relatively low intensity from the nitrogen lone pair to the π*(C=O) and Rydberg orbitals, respectively.

Structural distortions during the S_0–T_1 transition in glycine are rather different from those in the L-methionine molecule. The C=O bond is more strongly prolonged, but the C–O link is compressed (Table S4, ESI†) compared with that in Table S1 (ESI†). The C–C bond becomes weaker and the C–N bond becomes shorter, whereas in L-methionine, the opposite distortions are observed with negligible amplitudes (Table S1, ESI†). Explanations come from Table 3 and Fig. S3 (ESI†); the S_0–T_1 transition in glycine is almost pure HOMO–LUMO excitation with the charge transfer from the amino group to the carboxyl moiety, whereas, in methionine, the local n–σ* excitation of the sulfide group provides an additional contribution to the stronger S_0–T_1 absorption. Such differences are determined by the sulphur atom, which is a component of methionine, which contributes to the SOC matrix elements, increasing the transition probability.

The first vertical $S_0 \rightarrow T_1$ transition in a glycine molecule in vacuum represents the $n(N) \rightarrow \pi_y^*(C=O)$ transition type based on its orbital nature. Both orbitals are oriented along the y-axis, which is approximately perpendicular to the O–C–C–N plane (xz). The singlet S_1 excited state was also of the same HOMO–LUMO type (Table 3). The calculated absorption $S_0 \rightarrow S_n$ spectrum (Fig. S1, ESI†) corresponds to the observed offset.[3] The two vertically excited singlet ππ* states of the peptide group of glycine produce the two most intense absorption bands, known as NV1′ and NV2′ transitions, according to Mulliken's nomenclature.[20] Our calculation predicts their energies at 7.92 and 9.98 eV, slightly lower than the results of ref. 20 (8.10 and 10.20 eV, respectively). Our glycine structure does not support an exact C_s symmetry.

The most intense vibronic band of glycine phosphorescence (vertical $T_1 \rightarrow S_0$ transition) is predicted to possess a relatively long radiative lifetime (Table 4) with negligible quantum yield at room temperature. The great Stokes shift of 355.4 nm (Tables 3 and 4) and small energy gap for emission readily predict the effective non-radiative quenching of glycine phosphorescence, accounting for the Huang–Rhys parameters of the out-of-plane vibrations ($y = 0.57, 0.32$ and 0.41) for active modes $\nu_7 = 556$, $\nu_8 = 590$, and $\nu_{12} = 1123$ cm^{-1}. The zig-zag bending deformation $\nu_{16} = 1349$ cm^{-1}, strongly mixed with C=O stretching, produces a large contribution to the NRQ rate constant estimated by the method.[18,19] Even the relatively low SOC integral $\langle T_1|H_{SO}|S_0\rangle = 16.9$ cm^{-1} (Table S3, ESI†) does not suppress the calculated

Table 3 Characteristics of the vertical electronic transitions from the ground state of glycine

State	λ, nm	Oscillator strength, f	Contribution of orbitals to the transition	ΔE, eV
T_1	239.5	4.9×10^{-8}	HOMO → LUMO (81.25%) (n_N–π*–transition)	5.176
S_1	230.6	6.71×10^{-3}	HOMO → LUMO (93.00%) (n_N–π*–transition)	5.375
T_2	228.6	3.79×10^{-7}	HOMO−1 → LUMO (40.95%) (n_O–π*–transition)	5.423
			HOMO−1 → LUMO+1 (28.19%) (n_O–Ry*–transition)	
S_2	215.5	1.178×10^{-2}	HOMO → LUMO+1 (58.52%)	5.755
			HOMO → LUMO+2 (36.39%) (n_N–Ry*–transition)	

13346 | *Phys. Chem. Chem. Phys.*, 2025, **27**, 13340–13351

This journal is © the Owner Societies 2025

Table 4 Characteristics of the vertical electronic transitions of glycine in the T_1-state optimized geometry (emission)

State	λ, nm	$\tau(T_1)$, s	Oscillator strength, f	Contribution of orbitals to the transition	ΔE, eV
T_1	584.9	0.035	1.46×10^{-7}	HOMO−2 ← LUMO (1.04%) HOMO−1 ← LUMO (6.46%) HOMO ← LUMO (91.04%)	2.120
S_1	449.0	2.25×10^{-7}	1.35×10^{-2}	HOMO−1 ← LUMO (3.3%) HOMO ← LUMO (95.88%)	2.761
T_2	332.3	0.00075	2.21×10^{-6}	HOMO−2 ← LUMO (56.48%) HOMO−1 ← LUMO (37.64%)	3.731
S_2	292.9	5.4×10^{-7}	2.38×10^{-3}	HOMO−1 ← LUMO (95.08%) HOMO ← LUMO (3.40%)	4.233

NRQ rate constant ($k_{NR} = 2.4 \times 10^4$ s^{-1}). Thus, the radiative rate of glycine phosphorescence ($k_p = 2.86 \times 10^2$ s^{-1}) cannot compete with non-radiative quenching. Since the singlet S_1 state is orbitally similar to the lowest triplet (Table 4), their structure and vibronic pattern could also be similar. The fluorescence radiative rate constant ($k_f = 4.44 \times 10^6$ s^{-1}, Table 4) cannot compete with the spin-allowed non-radiative quenching rate,[22] which could be about 10^9 s^{-1} by similar vibronic reasons as those in triplet state quenching.[18,22] According to these estimations, glycine cannot produce photo-emission and all the absorbed ultraviolet energy (Fig. S1b, ESI†) must be transferred into the mutually hindered rotation of its functional groups.

Absorption spectrum of cysteine

The optimised cysteine geometry structures in the S_0 and T_1 states obtained using DFT and TD-DFT methods, respectively, are shown in Fig. 4. The ground state structure corresponds to the Ig$^-$g isomer detected by microwave spectra; its free energy is slightly higher at room temperature (by 299 cm^{-1}) than that of the most stable IIgg isomer, which is bound by three hydrogen bonds, as calculated by Barone et al.[18] Our structure is more flexible since it includes only two hydrogen bonds (C=O···HN···HS); thus, it easily relaxes after photoexcitation. The calculated rotational constants of the Ig$^-$g isomer[18] coincide with our data, with an accuracy of 0.003 cm^{-1}. The geometrical characteristics of the $S_0 \rightarrow T_1$ transition are presented in Table S5 (ESI†). The singlet–triplet transition is

Fig. 4 Optimized structure of the S_0 ground state (a) and T_1 excited state (b) of cysteine.

Table 5 Characteristics of the vertical electronic transitions of cysteine in the S_0-state optimized geometry (absorption)

State	λ, nm	Oscillator strength, f	Contribution of orbitals to the transition	ΔE, eV
T_1	268.3	4.00×10^{-6}	HOMO → LUMO (64.42%) HOMO → LUMO+1 (15.59%)	4.621
S_1	250.3	6.05×10^{-3}	HOMO → LUMO (89.17%) HOMO → LUMO+1 (4.25%)	4.953
T_2	248.2	1.10×10^{-5}	HOMO−2 → LUMO+1 (14.2%) HOMO−1 → LUMO (12.12%) HOMO−1 → LUMO+1 (15.6%) HOMO → LUMO (14.04%) HOMO → LUMO+1 (21.36%)	4.996
S_2	235.7	2.09×10^{-2}	HOMO → LUMO (5.10%) HOMO → LUMO+1 (85.57%)	5.260

accompanied by stretching of the C=O bond by 0.161 Å and by partial mutual rotation of the sulfide and amino groups (Fig. 4).

The $S_0 \rightarrow T_1$ transition is characterised by a 64.4% electron jump from the HOMO to the LUMO and by 15.6% as a HOMO–LUMO+1 transition. The highest occupied MO for cysteine refers to the localization of a lone pair of electrons of the sulfur atom at $4p_y$ AO (Fig. S5, ESI†). According to Table 5, the vertical $S_0 \rightarrow T_1$ transition in the gas phase is intense and has an oscillator strength of $f = 4.00 \times 10^{-6}$. In addition, the common trend of the tendency that the $S_0 \rightarrow T_2$ transition is an order of magnitude more intense than the $S_0 \rightarrow T_1$ transition is repeated again, as in previous examples.

These theoretical calculations indicate that the electronic spectrum of cysteine is located in the same ultraviolet region as that of methionine (Fig. S1c, ESI†). The band half-width in Fig. S1 (ESI†) is equal to 0.61 eV. The spectrum exhibited a peak at 200 nm that subsequently decreased in intensity, reaching 270 nm. At 235.7 nm, a secondary threshold is discernible, which, in theory, corresponds to the $S_0 \rightarrow S_2$ transition with an oscillator strength of $f = 2.09 \times 10^{-2}$.

The probability of the first triplet–singlet transition in sulfur-containing amino acids is influenced by the SOC term in eqn (4). The theoretically determined SOC ME integral $\langle T_1|H_{SO}|S_0\rangle$ for cysteine is equal to 90.87 cm^{-1}. This leads to the mixing of states with different multiplicity, thus mitigating forbidden transitions. In consideration of the spin–orbit coupling for the vertical $S_0 \rightarrow T_1$ transition, the theoretical lifetime of the first excited state T_1 of cysteine was determined to be 0.27 ms (Table S1, ESI†). This radiative triplet state parameter
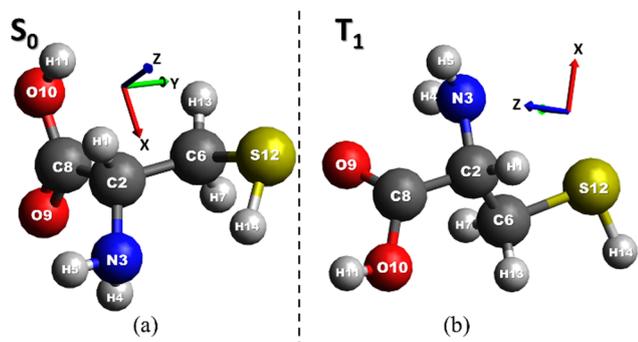
This journal is © the Owner Societies 2025

Phys. Chem. Chem. Phys., 2025, **27**, 13340–13351 | **13347**

Table 6 Characteristics of the vertical electronic transitions of cysteine in the T_1-state optimized geometry (emission)

State	λ, nm	$\tau(T_1)$, s	Oscillator strength, f	Contribution of orbitals to the transition	ΔE, eV
T_1	661.0	0.0056	1.18×10^{-6}	HOMO$-2 \leftarrow$ LUMO (19.24%)	1.876
				HOMO$-1 \leftarrow$ LUMO (5.16%)	
				HOMO $\leftarrow$ LUMO (74.21%)	
S_1	557.6	1.16×10^{-5}	4.02×10^{-4}	HOMO$-2 \leftarrow$ LUMO (6.72%)	2.224
				HOMO$-1 \leftarrow$ LUMO (4.65%)	
				HOMO $\leftarrow$ LUMO (88.31%)	
T_2	456.9	0.0024	1.30×10^{-6}	HOMO$-3 \leftarrow$ LUMO (14.48%)	2.713
				HOMO$-2 \leftarrow$ LUMO (42.20%)	
				HOMO$-1 \leftarrow$ LUMO (22.64%)	
				HOMO $\leftarrow$ LUMO (18.73%)	
S_2	403.5	1.09×10^{-7}	2.25×10^{-2}	HOMO$-2 \leftarrow$ LUMO (7.17%)	3.073
				HOMO$-1 \leftarrow$ LUMO (84.21%)	
				HOMO $\leftarrow$ LUMO (8.13%)	

in the ground-state geometry has a limited physical meaning, so we calculated the phosphorescence properties at the optimized triplet T_1 state structure for the vertical $T_1 \rightarrow S_0$ emission (Table 5 and Fig. S6, ESI†).

We predict visible emission at 661 nm with a radiative lifetime of 5.6 ms for the $T_1 \rightarrow S_0$ vertical transition of cysteine in the T_1-state optimized geometry. A great Stokes shift (392.7 nm, Tables 5 and 6) is predicted for this most intense (vertical) phosphorescence band, which produces a return from the $\nu' = 0$ global upper state to the combinations of a few ν'' vibrational quanta of the ground electronic state for the quasi-resonance energy conditions (Fig. S9, ESI†). Such a vertical transition can be accompanied by vibrational quanta excitations. The energy flow to these large nuclear displacements effectively transfers electronic triplet state excitation to the heating of the local environment. Like in other amino acids, a large Stokes shift and a small $E(T_1)$–$E(S_0)$ energy gap (1.87 eV) lead to fast non-radiative quenching of cysteine phosphorescence, accounting for the great flexibility of the branched σ-core with rather different force fields in the triplet and singlet states. A relatively large $\langle T_1|H_{SO}|S_0\rangle$ matrix element finally provides an intersystem crossing (ISC) rate constant higher than 4.65×10^7 s^{-1}. Comparison with the radiative rate constant ($k_p = 1.78 \times 10^2$ s^{-1}) predicts complete quenching of cysteine phosphorescence in any biological solvent.

It is interesting to estimate the hypothetical 0–0 phosphorescence band wavelength of cysteine as a possible photophysical reference point (without calculation of its Franck–Condon

factor, which is supposed to be close to unity). The total electronic energy of the S_0 and T_1 optimized states of cysteine is equal to -721.82085 and -721.74272 a.u., respectively; thus, the electronic adiabatic transition energy is 2.126 eV, which corresponds to 583.2 nm. The vibrational zero-point energy of the S_0 and T_1 optimized states is 0.10712 and 0.10324 a.u., respectively. It is predicted that the 0–0 phosphorescence transition energy will be 2.02 eV, which is equivalent to a 613.8 nm emission in the dark red region. These parameters can be used as theoretical molecular constants applicable for energy transfer estimation. However, we believe that there is no chance of observing such a weak emission band.

Tryptophan fluorescence and the possible role of the triplet state

Among the three aromatic amino acids that produce fluorescence, tryptophan (TRP) emission is particularly useful because it typically has a large cellular concentration (up to 3% in membranes), intense light absorption and relatively high fluorescence quantum yield (0.2).[23] Tryptophan fluorescence spectroscopy is often used to obtain structural information about intracellular environments by studying solvent quenching effects. However, the involvement of the TRP triplet state in fluorescence quenching via the ISC mechanism has not been reported in the literature.[23–25]

In Table 7, we present our TD-DFT results for the vertical absorption spectrum of tryptophan in ground S_0-state geometry

Table 7 TD-DFT results for the vertical absorption spectra of tryptophan in the ground S_0-state geometry

State	λ, nm	f	Configuration state function	E, eV
T_1	370.1	2.60×10^{-8}	$-0.95(54{-}55) - 0.15(52{-}55) - 0.13(53{-}60)$	3.35
T_2	276.9	3.74×10^{-9}	$-0.94(53{-}55) + 0.16(53{-}56)$	4.04
T_3	269.0	2.56×10^{-7}	$0.60(54{-}56) - 0.32(51{-}55) - 0.43(54{-}60)$	4.48
S_1	266.0	0.0842	$0.89(54{-}55) - 0.26(54{-}56) + 0.19(53{-}60)$	4.61
S_2	266.7	0.0070	$0.95(54{-}56) + 0.24(54{-}55)$	4.65
S_3	256.7	0.0317	$0.68(53{-}55) + 0.40(54{-}57)$	4.83
S_4	255.1	0.0143	$-0.86(54{-}57) + 0.32(53{-}55)$	4.86
S_5	246.0	0.0142	$+0.91(54{-}58) + 0.21(54{-}59)$	5.04
S_6	240.8	0.0041	$0.96(54{-}59) + 0.19(54{-}58) - 0.13(53{-}56)$	5.15
S_7	236.6	0.0032	$-0.89(53{-}57) + 0.35(52{-}55)$	5.24
S_8	236.2	0.0047	$-0.86(52{-}55) - 0.35(53{-}56) - 0.21(52{-}57)$	5.25
S_9	227.9	0.0069	$0.95(54{-}61) - 0.20(54{-}58)$	5.44

13348 | *Phys. Chem. Chem. Phys.*, 2025, **27**, 13340–13351

This journal is © the Owner Societies 2025

for the singlet and triplet excited states while accounting for the SOC perturbation. Table 7 predicts relatively intense $S_0 \rightarrow S_1$ absorption and fluorescence, in good agreement with the experimental data.[23] The calculated oscillator strength ($f = 0.084$) well corresponds to the observed molar extinction coefficient ($\varepsilon = 5600$ L mole^{-1} cm^{-1}).[24] The indole moiety of tryptophan is commonly assumed to be the main source for the ultraviolet absorbance of proteins at 270–280 nm and for their fluorescence at 350 nm.[23–26] The two closely lying states S_1 and S_2 with their different dipole moments can interchange relative energy positions depending on solvent polarity.[25] The S_2 state is more stabilized in polar solvents and produces fluorescence, whereas emission originates from the S_1 state in nonpolar environments.[25] The S_2 state is determined by the HOMO $\rightarrow$ LUMO+1 transition (54–56, Table 7), which represents a pure charge transfer from the delocalized indole π-HOMO to the Rydberg orbital at the N_{11} atom (Fig. S10 and S11, ESI†). The S_1 state represents 79% of the HOMO $\rightarrow$ LUMO excitation, which is a $\pi \rightarrow \pi^*$ transition inside the indole moiety (Fig. S11, ESI†). The permanent dipole moment (4.22 Debye) was similar to that of the ground S_0 state (4.05 Debye). This is the reason for the absence of a strong solvato-chromic effect in the S_0–S_1 transition.

The triplet state of tryptophan represents 90% of the same HOMO $\rightarrow$ LUMO transition; Fig. S10 (ESI†) indicates that this is a $\pi \rightarrow \pi^*$ excitation in the aromatic part of the molecule with a very small contribution of charge-transfer from the amino group to the indole moiety. We suspect that the T_1 state of tryptophan could be an intermediate step in energy dissipation because of its long radiative lifetime (0.079 s, Table S3, ESI†) and high flexibility with respect to the mutual internal rotation of carboxyl and amino groups, which is involved through the charge-transfer contribution to electronic-vibrational relaxation. The solvent-dependent energy gap between the S_2 and S_1 states strongly influences the ISC rate constant for the generation of the T_1 state of tryptophan; thus, it governs the efficient rate of fluorescence quenching. The tryptophan fluorescence wavelength (λ_{max}) and emission intensity are strongly affected by the polarity of the peptide microenvironment.[25]

The S_1 state is orbitally similar to the triplet T_1 state function; however, there are some differences in the charge-transfer admixtures (Table 7 and Fig. S11, ESI†). A small admixture (2.5%) to the $S_0 \rightarrow T_1$ vertical transition of the HOMO–2 $\rightarrow$ LUMO excitation (52–55) provides a pure charge transfer from the amino group to the indole moiety (Fig. S11, ESI†). The T_1 state of tryptophan, as with other aromatic triplets, has relatively low excitation energy and low oscillator strength ($f \approx 10^{-8}$); its weak absorption must be observed in the near-UV region. Because of the CT admixture from the non-planar peptide fragment with its n-orbitals of lone pairs, tryptophan exhibits more intense $S_0 \rightarrow T_1$ absorption than the pure indole molecule.[10] However, it is still predicted to be rather weak and the absence of experimental data about such absorbance indirectly supports our findings: an absorption band with $f \approx 10^{-8}$ is impossible to detect below noise using standard UV spectrometers. However, time-dependent EPR or

optically detected magnetic resonance measurements in cold crystals can shed light on triplet tryptophan properties. Accounting for the importance of tryptophan fluorescence as an indicator of protein structure, T_1 detection could open new channels for the regulation of TRP emission and intermolecular energy-transfer mechanisms. The long radiative lifetime of triplet tryptophan (Table S3, ESI†) provides additional opportunities for such regulation, including the ways of studying UV radiation damage in proteins.

The experimentally well-studied fluorescence of tryptophan is a good anchor for the continuation of our study on SOC effects in amino acids and their triplet-state properties.

Conclusions

A detailed analysis of the electronic spectra of a few amino acids was performed in this work, using time-dependent density functional theory with the inclusion of spin–orbit coupling (SOC) perturbation. The electronic vertical absorption and emission spectra were obtained, and the probabilities of forbidden singlet–triplet transitions were predicted. These results offer a novel perspective on the photobiology of amino acids because they predict the important role of the ''dark'' T_1 excited state in the UV photolysis of proteins. First, the SOC matrix elements in the aliphatic amino acids responsible for promoting the $S_0 \rightarrow T_1$ transition intensity are orders of magnitude larger than the SOC parameters in the aromatic counterparts like tryptophan. This SOC contribution influences the ZFS parameters in the EPR spectra and S–T transitions probability of radiative and non-radiative types, including the effective luminescence quenching of aliphatic amino acids through various ISC and IC processes.

For the vertical $S_0 \rightarrow T_1$ transition in L-methionine, we predict an absorption maximum at 260 nm with an oscillator strength $f = 2.76 \times 10^{-6}$. Such molar extinction (about $\varepsilon \approx 1$–10 M^{-1} cm^{-1}) could be measurable by spectrometers with a long optical path.

The large torsional and bond-length distortions during the S_0–T_1 transitions in aliphatic amino acids explain the effective quenching of their phosphorescence, under account for a big SOC integral and a small energy gap in the optimized triplet state geometry. The great Stokes shift of 345 nm is predicted for methionine emission supporting its quenching mechanism by energy transfer to intramolecular vibrations, including mutual twisting of all functional groups, rocking and scissoring movements mixed with valence C=O distortions. The orbitally similar S_1 state can form the conical intersection with the ground state, which leads to fluorescence quenching for similar reasons. Glycine differs from sulfur-containing amino acids by a smaller SOC integral ($\langle T_1|H_{SO}|S_0\rangle = 16.7$ cm^{-1}), which is still much higher than that of aromatic molecules. Such SOC estimation is typical for many other aliphatic peptide molecules. One can predict that the onset of protein UV absorption must be determined by the $S_0 \rightarrow T_1$ vertical transition of the $n(N) \rightarrow \pi_y^*(C=O)$ transition type according to its orbital

This journal is © the Owner Societies 2025

Phys. Chem. Chem. Phys., 2025, **27**, 13340–13351 | **13349**

nature; that is, a charge transfer (CT) from the amine lone pair to the carbonyl group. This is a more intense S–T absorption than that of many other organic molecules. This onset corresponds to 260 nm (similar to glycine) and encompasses almost all amino acid residues in the protein scaffold.

UV light absorption in the 250–260 nm range may produce direct excitation of the two lowest triplet excited states T_1 and T_2, which could start radiolysis of amino acids since the T_1 state in all studied molecules is quite unstable (especially in the sulfur-containing amino acids).

Tryptophan, which is the most important UV absorber and emitter in proteins, also does not exhibit triplet-state manifestations. The $S_0 \rightarrow T_1$ transition represents $\pi \rightarrow \pi^*$ excitation in the aromatic moiety with a small admixture of CT from the amino group to indole; its weak absorption ($f \approx 10^{-8}$) occurs in the near-UV region at 370 nm. A series of low-lying triplet states is important for the quenching mechanism of tryptophan fluorescence.

Author contributions

Boris Minaev: writing – review & editing, writing – original draft, data curation, conceptualization. Maryna Sukhyna: data curation. Pavlo Stakhira: data curation. Valentina A. Minaeva: validation, methodology. Hans Ågren: writing – review & editing.

Data availability

The data supporting this article have been included as part of the ESI.†

Conflicts of interest

The authors declare that they have no known competing financial interests or personal relationships that could have appeared to influence the work reported in this paper.

Acknowledgements

Notes and references

1 G. Baryshnikov, B. Minaev and H. Ågren, Theory and Calculation of the Phosphorescence Phenomenon, *Chem. Rev.*, 2017, **117**, 6500–6537.

2 C. A. Parker, *Photolumlnescence of Solutions*, American Elsevier, New York, 1968.

3 G. D. Fasman, *Practical Handbook of Biochemistry and Molecular Biology*, CRC Press, 1992.

4 B. Minaev, O. Lut, G. Baryshnikov and V. Minaeva, Calculation of structure and spectra of the glycine radical with dehydrogenated carboxyl group, *Ukr. Bioorg. Acta*, 2009, **2**, 35–41.

5 A. Acharya, A. M. Bogdanov, B. L. Grigorenko, K. B. Bravaya, A. V. Nemukhin, K. A. Lukyanov and A. I. Krylov, Photo-induced Chemistry in Fluorescent Proteins: Curse or Blessing?, *Chem. Rev.*, 2017, **117**, 758–795, DOI: **10.1021/acs.chemrev.6b00238**.

6 R. B. Vegh, K. M. Solntsev, M. K. Kuimova, S. Cho, Y. Liang, B. L. Loo, L. M. Tolbert and A. S. Bommarius, Reactive oxygen species in photochemistry of the red fluorescent protein "Killer Red", *Chem. Commun.*, 2011, **47**, 4887–4889.

7 V. Carravetta, O. Plashkevich and H. Ågren, A theoretical study of the near-edge x-ray absorption spectra of some larger amino acids, *J. Chem. Phys.*, 1998, **109**, 1456–1464, DOI: **10.1063/1.476696**.

8 B. F. Minaev, Quantum-chemical investigation of the mechanisms of the photosensitization, luminescence, and quenching of singlet $^1\Delta_g$ oxygen in solutions, *J. Appl. Spectrosc.*, 1985, **42**, 518–523.

9 H. Ågren, O. Vahtras and B. Minaev, *Advances in Quantum Chemistry*, ed. P.-O. Löwdin, J. R. Sabin and M. C. Zerner, Academic Press, 1996, vol. 27, pp. 71–162.

10 Ó. Rubio-Pons, O. Loboda, B. Minaev, B. Schimmelpfennig, O. Vahtras and H. Ågren, CASSCF calculations of triplet state properties: applications to benzene derivatives, *Mol. Phys.*, 2003, **101**, 2103–2114.

11 F. Sang, X. Zhang and F. Shen, Fluorescent methionine-capped gold nanoclusters for ultra-sensitive determination of copper(II) and cobalt(II), and their use in a test strip, *Microchim. Acta*, 2019, **186**, 1–9, DOI: **10.1007/s00604-019-3428-3**.

12 F. Neese, *Wiley Interdiscip. Rev.: Comput. Mol. Sci.*, 2012, **2**, 73–78.

13 A. D. Becke, A new mixing of Hartree–Fock and local density-functional theories, *J. Chem. Phys.*, 1993, **98**, 1372–1377.

14 R. Krishnan, J. S. Binkley, R. Seeger and J. A. Pople, Self-consistent molecular orbital methods, XX. A basis set for correlated wave functions, *J. Chem. Phys.*, 1980, **72**, 650–654.

15 M. Kinoshita, N. Iwasaki and N. Nishi, Molecular Spectroscopy of the Triplet State through Optical Detection of Zero-Field Magnetic Resonance, *Appl. Spectrosc. Rev.*, 1981, **17**, 1–94.

16 B. Minaev, O. Loboda, O. Vahtras, K. Ruud and H. Ågren, Solvent effects on optically detected magnetic resonance in triplet spin labels, *Theor. Chem. Acc.*, 2004, **111**, 168–175.

17 S. Gunasekaran, A. Bright, T. Renuga Devi, R. Arunbalaji and G. Anand, Experimental and Semi-empirical computations of the vibrational spectra of Methionine, Homocysteine and Cysteine, *Archiv. Phys. Res.*, 2010, **1**, 12–26.

18 R. R. Valiev, R. T. Nasibullin, V. N. Cherepanov, G. V. Baryshnikov and D. Sundholm, *et al.*, First-principles calculations of anharmonic and deuteration effects on the photophysical properties of polyacenes and porphyrinoids,

13350 | *Phys. Chem. Chem. Phys.*, 2025, **27**, 13340–13351

This journal is © the Owner Societies 2025

Phys. Chem. Chem. Phys., 2022, **22**(39), 22314–22323, DOI: **10.1039/d0cp03231j**.

19 G. V. Baryshnikov, R. R. Valiev, N. N. Karaush, V. A. Minaeva and A. N. Sinelnikov, *et al.*, Benzoannelated aza-, oxa- and azaoxa[8]circulenes as promising blue organic emitters, *Phys. Chem. Chem. Phys.*, 2016, **18**(40), 28040–28051.

20 L. Serrano-Andres and M. P. Fulscher, Theoretical Study of the Electronic Spectroscopy of Peptides. 2. Glycine and *N*-Acetylglycine, *J. Am. Chem. Soc.*, 1996, **118**, 12200–12206, DOI: **10.1021/ja9619972**.

21 V. Barone, M. Fusè, F. Lazzari and G. Mancini, Benchmark Structures and Conformational Landscapes of Amino Acids in the Gas Phase: A Joint Venture of Machine Learning, Quantum Chemistry, and Rotational Spectroscopy, *J. Chem. Theory Comput.*, 2023, **19**, 1243–1260.

22 L. Shi, X. Xie and A. Troisi, Rapid calculation of internal conversion and intersystem crossing rate for organic materials discovery, *J. Chem. Phys.*, 2022, **157**, 134106, DOI: **10.1063/5.0102857**.

23 C. J. Fossum, B. O. V. Johnson and S. T. Colde, *et al.*, Insights into the Mechanism of Tryptophan Fluorescence Quenching due to Synthetic Crowding Agents: A Combined Experimental and Computational Study, *ACS Omega*, 2023, **8**, 44820–44830, DOI: **10.3390/ijms151222518**.

24 F. W. J. Teale and G. Weber, Ultraviolet fluorescence of the aromatic amino acids, *Biochem. J.*, 1957, **65**, 476–482.

25 A. B. T. Ghisaidoobe and S. J. Chung, Intrinsic Tryptophan Fluorescence in the Detection and Analysis of Proteins: A Focus on Förster Resonance Energy Transfer Techniques, *Int. J. Mol. Sci.*, 2014, **15**, 22518–22538, DOI: **10.3390/ijms151222518**.

26 A. Lindinger, J. P. Toennies and A. F. Vilesov, High resolution vibronic spectra of the amino acids tryptophan and tyrosine in 0.38 K cold helium droplets, *J. Chem. Phys.*, 1999, **110**, 1429–1436, DOI: **10.1063/1.478018**.

This journal is © the Owner Societies 2025

Phys. Chem. Chem. Phys., 2025, **27**, 13340–13351 | **13351**